OBLIQUE-INCIDENCE UT INSPECTION OF DIFFUSION BONDS

F. J. Margetan, R. B. Thompson, and T. A. Gray

Ames Laboratory, USDOE
Iowa State University
Ames, IA 50011

INTRODUCTION

An increasingly important metal joining procedure is based on "solid-state bonding", which employs the application of temperature and stress to a metal-metal interface. Under ideal conditions[1], a sequence of metallurgical processes produces a bond whose mechanical properties are identical to those of the host material. This sequence involves the deformation of the interfaces to achieve intimate mechanical contact, atomic diffusion to achieve the "solid-state" bonding, and grain growth to remove the microstructural memory of the original interface. Standard NDE techniques can be used to detect discrete flaws in the bonds. However, even in the absence of discrete flaws, strength and fatigue resistance may be degraded by subtle differences between the microstructures of the interface region and the bulk material. This paper is motivated by a particular bonding process (diffusion bonding as applied to aircraft engine rotor components), and considers only one metallurgical cause of weak bonding (distributions of microscopic pores in the bond plane). Figure 1 presents a model problem which has been chosen to simulate the inspection of such bonds as they occur when turbine blades are joined to hubs. The model geometry consists of two rectangular plates of similar material which have been diffusion bonded in the xy plane. The bond plane is assumed to contain an array of circular cracks characterized by s, the center-to-center separation of adjacent cracks, and by A, the fraction of the area in the xy plane that is composed of cracks. It is assumed that the bonded part is submerged, and that a corner reflection is used to examine the incomplete bond. A typical ultrasonic ray is shown leaving a transmitting transducer, undergoing a corner reflection, and returning to a receiving transducer. Mode conversion may have occurred at any of the transmission or reflection points, so $\Theta = \Theta'$ and $\phi = \phi'$ need not hold.

In the following section, we describe eight categories of specular corner reflections, and we illustrate how time-of-flight can be used to partially distinguish these experimentally. We then present model calculations for the intensity of the outgoing wave in water, and we demonstrate their use in optimizing the choices of reflection category and inspection angle. Preliminary comparisons of theory to experiment are then presented for diffusion-bonded specimens of IN100, a nickel-based superalloy. One ingredient in our calculations is the quasi-static distributed-spring (DS) model[2-5] for the reflection of sound from an imperfect interface. Mathematically, the interface is represented by a distribution of ideal springs connecting the two unflawed halves of the specimen. The effective longitudinal and transverse spring stiffness constants are estimated from stress intensity factors[2,5,6]. These spring constants appear in boundary equations which are solved to obtain the reflection and transmission coefficients for plane waves incident on the imperfect interface.

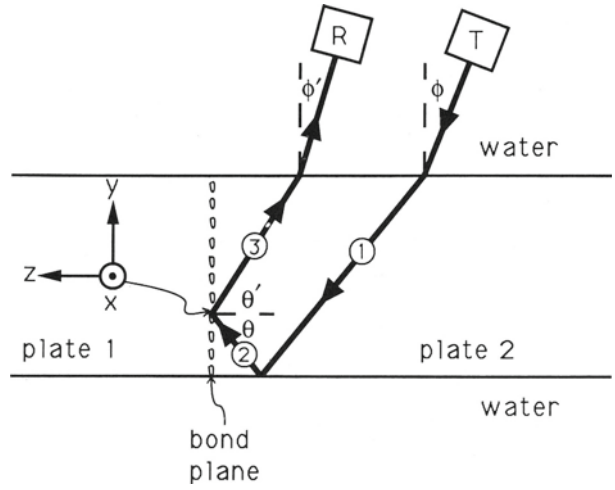

Fig. 1. Inspection geometry and model coordinate system.

In applying the DS model to dynamic scattering problems, we assume that the wavelength (λ) of the interrogating sound is large compared to the interface structure (s). Details of the DS model calculations, and general features of the solutions can be found in Ref. 5. That work also treats strip-like cracks, and considers several other metals in addition to IN100.

CATEGORIES OF CORNER REFLECTIONS

Consider the case in which the transmitting probe emits an ultrasonic pulse of short duration, and assume that the plate being inspected is sufficiently thick that the corner-reflected pulse arriving at the receiver is cleanly separated in time from later arriving reverberations. The incident pulse may be represented as a superposition of plane waves, and in the ensuing discussion we follow one of these plane wave components as it undergoes the corner reflection. For the inspection geometry of Fig. 1 with an incident compressional plane wave in water, particle displacements in both the water and the solid will have no x-components. The most general particle motion in the solid will then be a combination of longitudinal (L) and transverse (T) waves with polarizations in the yz plane. The soundpath within the solid contains three legs, and these have been labelled (1), (2), and (3) in Fig. 1. Because mode conversion can occur at each transmission and reflection point, each leg can be traversed by either longitudinal or transverse sound waves. There are eight distinct ways of assigning wave types to the three legs, namely (1)(2)(3) = LLL, LLT, LTL, LTT, TLL, TLT, TTL, and TTT. We refer to these as the eight categories of corner reflections. Eight additional categories could be enumerated by considering cases in which the incident ray in the solid first reflects from the bond plane. The ray paths for these cases may be obtained by reversing the directions of the arrows in Fig. 1., i.e., by interchanging the roles of the two transducers. However, the reciprocity principle implies that interchanging the transmitting and receiving probes can have no effect on the received signal. Thus it is sufficient to consider the ray sequence shown in Fig. 1, and the eight corner reflection categories enumerated above.

At each interface in Fig. 1, including the bond plane, the angles of the incident and outgoing plane waves are restricted if propagating wave solutions are to exist along all legs of the sound path. One finds[5] that the LTL category is generally forbidden from occurring, but the other seven categories are each allowed for some range of the incident water angle ϕ. One finds that $\phi' = \phi$ (one requirement for single-probe inspections) for the LLL, TTT, LTT and TLL categories, and that $\phi' \neq \phi$ for TLT, TTL and LLT. For an incident steady-state plane wave at a given value of ϕ, several corner-reflection categories may be

allowed, and all would be simultaneously present within the solid. However, corner-reflected signals belonging to different categories may have significantly different transit times through the solid, and time-of-flight observations can be used to separate such signals when sound pulses of short duration are used.

The use of time-of-flight to experimentally separate corner-reflection categories is demonstrated in Fig. 2. In this case, a single focussed transducer was used to inspect a poorly-bonded submerged specimen of IN100. Prior to t=0 the probe had emitted a pulse of ultrasound, and Fig. 2 displays the subsequent echoes returning to the probe as a function of time. When the probe was positioned far from the bond region (Fig. 2a), one observed a large amplitude echo from the front surface of the plate, and a smaller, later echo from the back surface. When the probe was positioned near the bond and scanned in the z-direction, a series of corner-reflected signals were observed (Fig. 2b). Different horizontal positions of the probe (i.e. different values of the probe's z-coordinate) were required to maximize the received signals for the different corner reflection categories. Direct back-surface reflection and grain scattered reflection are two common sources of background signals having times-of-flight similar to the corner-reflection signals being sought. The back surface reflection primarily impacts the LLL inspection at small angles of incidence, while grain scattering can affect all categories.

INSPECTION OPTIMIZATION

In principle, any category of corner-reflection can be used to detect imperfect diffusion bonds in the geometry of Fig. 1. In practice, the categories resulting in the largest received signals or best signal-to-noise ratios would be preferred. To this end, the DS model can be used to guide the selection of inspection category, illumination angle and frequency. The model predicts bond reflectivity to increase with increasing frequency; thus, the inspection frequency should be chosen as high as possible subject to the constraint that grain scattering from the base material or heat-affected zone is not too great. Broadband transducers are preferable, as they allow the characteristic rise of reflectivity with frequency to be observed, a feature which may be used to differentiate bond signals from spurious signals. Such damped transducers also allow the various signals to be resolved in time. The remainder of this section deals with the optimization of the corner-reflection category and illumination angle at a fixed frequency.

Our methodology is to postulate a hypothetical disbond distribution in a bonded specimen, assume an incident plane wave in water of given amplitude, frequency and illumination angle, and then to calculate the amplitudes of the outgoing water waves for each corner-reflection category. By repeating such calculations for various disbond distributions, one can discover the categories and illumination angles which give rise to the largest outgoing amplitudes. The most rigorous calculation would incorporate diffraction and beam spread effects by explicitly including the geometrical parameters of the transducer. One possible approach would be to represent the incident beam as an angular spectrum of plane waves. Each plane wave component could be followed through the corner-reflection process, and the components could be summed at the surface of the receiver. This general approach will be deferred to a subsequent publication. Here the results for a single plane wave component will be examined, and we will use a figure of merit based on outgoing wave intensities to compare the corner reflection categories. An alternative figure of merit based on outgoing wave energies is also used in Ref. 5. Let U_0 denote the displacement amplitude of the incident plane wave in water, and let U_{out} denote the displacement amplitude of the wave reflected from the corner after it has passed from the solid back into the water. For a given category, the ratio U_{out}/U_0 may be calculated as the product of two transmission and two reflection coefficients, the reflection coefficient for the bond being obtained using the DS model. Experimentally, it is convenient to relate the strengths of the various corner-reflected waves to that of a calibration signal. Here, the calibration amplitude (U_{cal}) is chosen to result from a back surface reflection at normal incidence (see the upper portion of Fig. 3).

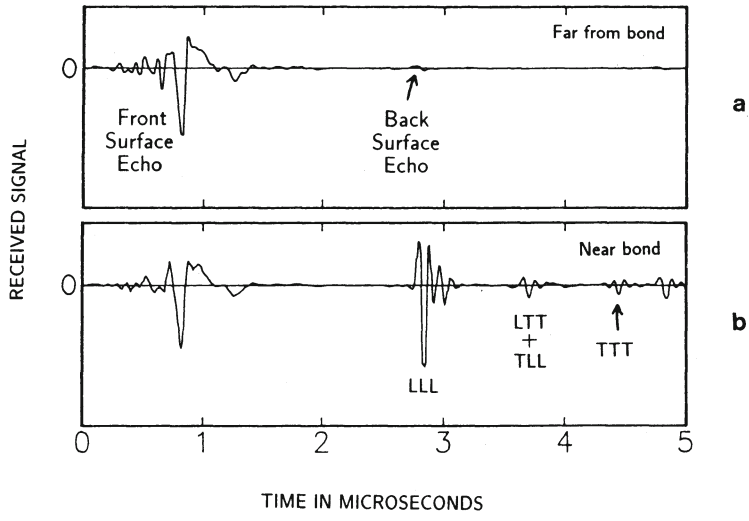

Fig. 2. Received voltage (arbitrary units) as a function of time for a pulse-echo inspection of a 0.64 cm thick diffusion-bonded IN100 specimen. A broadband transducer having a 1.27 cm diameter, a 7.6 cm focal length in water, and a 15-MHz center frequency was used. For the central ray from the transducer, $\phi = 6°$ and the one-way waterpath was 5 cm. (a): Received signal with transducer positioned far from the bond plane. (b): Received signal with transducer positioned near the bond plane.

The results of a typical series of corner-reflection calculations are displayed in Fig. 3. There we have assumed a submerged specimen of IN100 illuminated using 15-MHz plane waves. The bond plane is assumed to contain an array of circular cracks having a 50μm spacing and a 20% total cracked area. For each of the seven allowed corner-reflection categories, the outgoing intensity in water is displayed as a function of the illumination angle ϕ. This corner intensity in decibels, CI, is defined as

$$CI = 10 \log_{10} |U_{out}/U_{cal}|^2 . \quad (1)$$

As ϕ increases from zero, the highest intensity signals are seen to occur for the LLL, TLL, TTT, and TTL categories in turn. These corner-reflected intensities are generally 30 to 40 dB below the calibration intensity for this rather well-bonded specimen. The LLL intensity is greatest when the water angle is small so that the L-waves subsequently approach the bond at near grazing incidence. In principle, the LLL detectability of the bond increases as ϕ decreases. In practice, LLL inspections with focussed probes typically require $\phi \geq 5°$ depending on the probe diameter and focal length; at smaller angles there can be a significant direct back-surface echo which will interfere with or mask the bond signal. The shear wave inspection, TTT, dominates at intermediate angles and is optimized when shear waves in the metal reflect off of the bond at near-45° incidence. For IN100, $\Theta = 45°$ occurs at $\phi = 18.6°$ which can be seen to be slightly beyond the TTT maximum at $\phi = 16.3°$ in Fig. 3. At $\Theta = 45°$, the shear wave reflectivity is independent of the shear mode spring stiffness constant; thus 45°-TTT inspection, with its large outgoing intensity, offers a convenient method of determining the longitudinal stiffness parameter. At yet larger water angles, the TTL corner-reflection dominates. Here transverse waves are mode converted to longitudinal waves by the bond, and the L-waves emerge nearly parallel to the bond plane. For example, when $\phi = 23°$ in Fig. 3, the TTL exiting water angle is $\phi' = 5.2°$. Because of this severe angle mismatch, separate transmitting and receiving probes are required for proper TTL inspections.

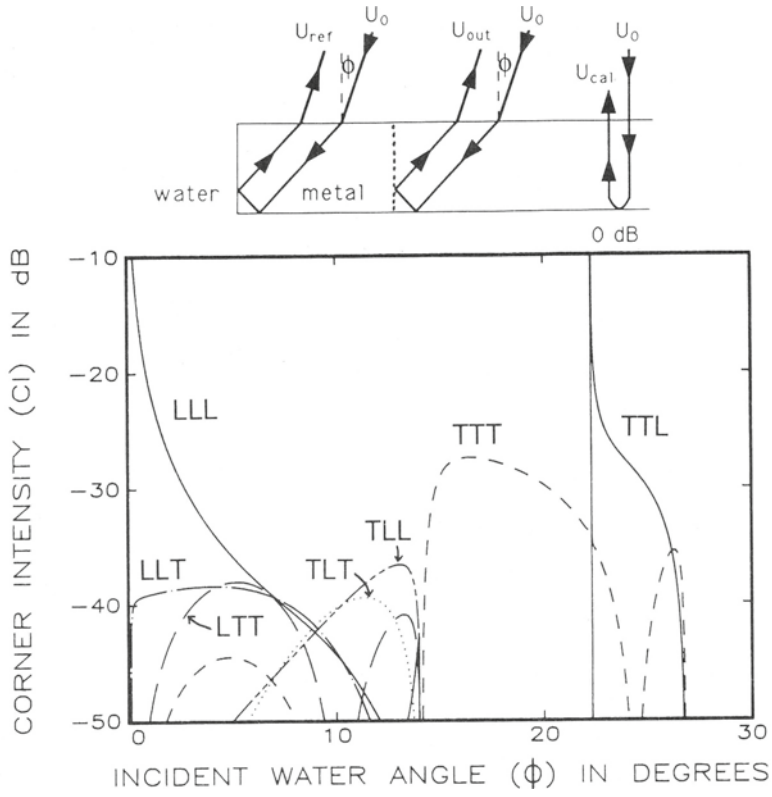

Fig. 3. Intensities of exiting 15 MHz plane waves in water following a corner reflection from a hypothetical diffusion bond in IN100. The bond plane is assumed to contain an array of circular cracks having s = 50μm and A = 0.2.

The IN100 results shown in Fig. 3 are for one choice of frequency and one choice of bond plane structure. For other choices one finds, to a first approximation, that the intensity curves maintain their shapes and relative positions, and simply shift together vertically on the figure. For a given illumination angle and inspection category, the relative intensity of the outgoing water wave is approximately proportional to the square of the frequency, the square of the crack spacing, and a power of the crack area fraction:

$$|U_{out}/U_{cal}|^2 \quad \propto \quad f^2 s^2 A^{2p} \tag{2}$$

where p = 3/2 and 2 for circular cracks and strip cracks respectively[5]. The approximate proportionality becomes exact in the limit of low crack area fraction. Thus in Fig. 3, if the frequency, disbond spacing, or crack area fraction were halved, the intensity curves would shift downward by approximately 6, 6, or 9 dB respectively. Note that low-frequency specular reflection experiments yield information about the product sA^p; such experiments cannot determine both s and A even when the crack shapes are known[5]. Because reflection and transmission coefficients depend upon material density and elasticity, the vertical ordering of the corner-reflected intensities can change when Fig. 3 is redrawn for different solids. However, in simulated inspections of bonds in a variety of metals, we again find that the LLL, TTT, and TTL reflections generally produce the largest outgoing intensities[5].

COMPARISON WITH EXPERIMENT

For focussed single-probe inspections of bonds in IN100, model calculations and reference experiments[5] predict that shear wave inspections TTT ($\phi \approx 18°$) will enjoy a significant advantage over L-wave inspections LLL ($\phi \approx 6°$). This advantage is predicted to range from about 15 dB for very poor bonds ($A \approx 1$) to about 7 dB for good bonds ($A \lesssim 0.4$). A series of bond inspections was made to test this prediction. Three 0.64 cm thick IN100 specimens, bonded using different temperature and pressure recipies to produce both good and degraded interfaces, were supplied to us by Pratt & Whitney. The bonds were classified as "good", "marginal", and "poor" by the manufacturer. After polishing and etching, microscopic examination of the upper and lower surfaces of the plates revealed no evidence of microcracks along the bond line in the "good" specimen, and intermittant bond-line microcracks in the other two specimens. In addition, the "poor" specimen exhibited a lengthy, nearly continuous crack near its center. The bond region of each specimen was inspected twice using the 15 MHz focussed probe of Fig. 2, once utilizing an LLL ($\phi = 6°$) corner-reflection, and once a TTT ($\phi = 18°$) reflection. For LLL inspections with this probe, an illumination angle of 6° was found to offer a reasonable compromise between high bond reflectivity and low back-surface-reflected background. In each inspection, the waterpath was chosen to focus the ultrasound near the back surface of the plate, and the probe was scanned parallel to this surface. The resulting C-scans, normalized by the back surface calibration signal are displayed in Figs. 4-6. The bond region appears as a ridge of high reflected amplitude running parallel to the x-axis of each graph.

For the "poorly bonded" specimen, the TTT and LLL C-scans can be seen to reveal similar patterns of peaks (poorly-bonded areas) and valleys (better-bonded areas) along the bond plane, as shown in Fig. 4. The large central peak occurs at the site of the continuous crack observed in the microscopic examination of the bond line. As expected

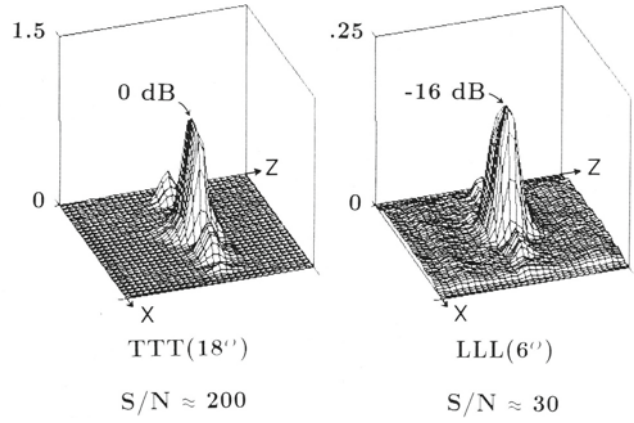

Fig. 4. Comparison of TTT($\phi = 18°$) and LLL($\phi = 6°$) pulse-echo inspections of a poorly-bonded IN100 plate using a focussed 15-MHz transducer. On the vertical axis we plot the peak-to-peak output voltage from the received corner-reflected signal divided by that of the back-surface calibration signal. In addition, the peak amplitude in decibels and the signal/noise ratio are indicated. The region scanned has dimensions $(\Delta x)\cdot(\Delta z) = (3.56cm)\cdot(0.953cm)$. (See Fig. 1.) At the extreme values of x, the center of the probe is beyond the edges of the plate.

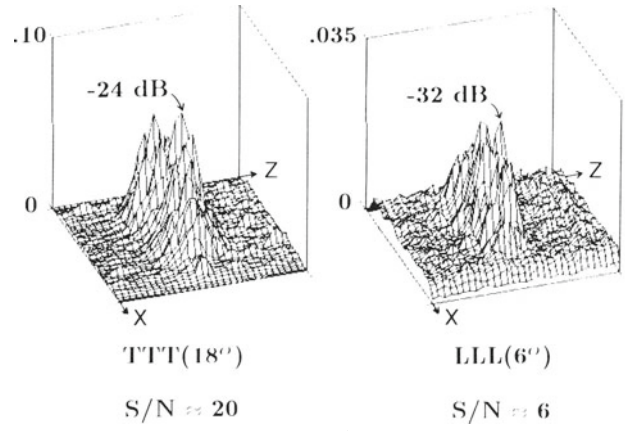

Fig. 5. Comparison of TTT and LLL inspections of a marginally well-bonded IN100 plate. See caption of Fig. 4.

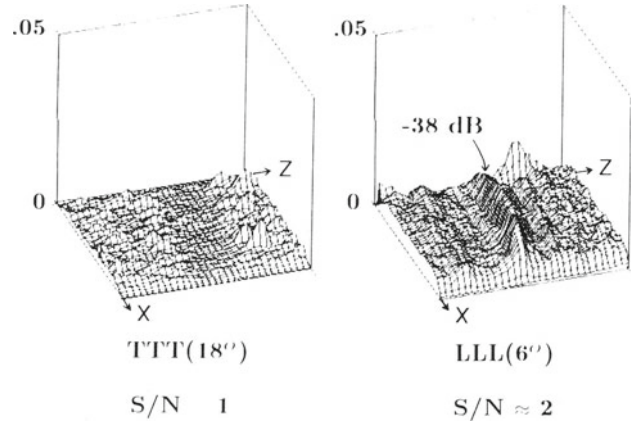

Fig. 6. Comparison of TTT and LLL inspections of a well-bonded IN100 plate. See caption of Fig. 4.

for a large single crack, the reflectivities of L and T waves from this region of the bond were found to be independent of frequency. In the "marginally" well-bonded sample, a somewhat more uniform corner-reflectivity was observed away from the sides of the specimen, as shown in Fig. 5. For each inspection method, this reflectivity was generally found to increase with frequency within the bandwidth of the transducer. As expected from Fig. 3 the shear wave inspection led to the larger received amplitudes in both the "poor" and "marginal" specimens. However, this was not the case for the "well-bonded" specimen, as shown in Fig. 6. There no evident TTT signal was seen, but a small LLL signal could be clearly discerned along the entire length of the bond. However, the bond reflectivity deduced from this LLL signal did not increase with frequency, and hence the signal is not consistent with scattering from a distribution of small disbonds. For the "poor" and "marginal" specimens, the TTT signal was not only larger than the LLL signal, but also had a significantly better signal-to-noise ratio. One would expect the shear waves with their smaller wavelength to suffer the greater grain scattering. However, grain-scattered background in these specimens at 15 MHz was not as significant as the back-surface-reflected background signal observed in the LLL inspection. This latter background signal has a visible effect on the LLL C-scans; it produces the plateau that is the lower limit of observed amplitude.

SUMMARY

In the preceeding sections, the quasi-static spring model was used to predict the frequency and angular dependence of the ultrasonic reflections from an imperfectly-bonded interface. Included were both shear and longitudinal wave reflection coefficients as well as coefficients governing the reflected mode-converted waves. This interface reflectivity model was incorporated into a corner-reflectivity model to predict the best configuration for inspecting diffusion bonds joining two abutting plates, a geometry which simulates one encountered in joining blades to rotors of turbine engine components. The model suggests that the measurement frequency should be as high as possible, subject to noise limitations. For single probe or pitch-catch measurements having $\phi' = \phi$, two preferred modes of inspection are indicated: using longitudinal waves, the geometry should be arranged so that the waves strike the interface at near grazing incidence; for shear waves, a near-45^{o} illumination of the interface was found to be preferred. Pitch-catch geometries having $\phi' \neq \phi$ can be used to detect mode-converted ($L \leftrightarrow T$) reflections from an imperfect interface; here the illumination angle should be chosen such that the incident or exiting L-wave propagates nearly parallel to the interface.

ACKNOWLEDGMENT

This work was sponsored by the Center for Advanced Nondestructive Evaluation, operated by the Ames Laboratory, USDOE, for the Air Force Wright Aeronautical Laboratories/Materials Laboratory under Contract No. W-7405-ENG-82 with Iowa State University.

REFERENCES

1. J. C. Lippold, Metallurgical characteristics and discontinuities in solid-state welds, Review of Progress in QNDE Vol. 8, D. O. Thompson and D. E. Chimenti, Eds., in press.
2. J. M. Baik and R. B. Thompson, Ultrasonic scattering from imperfect interfaces: a quasi-static model, J. Nondestr. Eval. 4: 177-196 (1984).
3. Y. C. Angel and J. D. Achenbach, Reflection of ultrasonic waves by an array of microcracks, Review of Progress in QNDE, 4A, D. O. Thompson and D. E. Chimenti, Eds., (Plenum Press, New York, 1986), p. 83.
4. T. A. Gray, F. J. Margetan, and R. B. Thompson, Ultrasonic NDE techniques for integrally fabricated rotors, Review of Progress in QNDE, 7B, D. O. Thompson and D. E. Chimenti, Eds., (Plenum Press, New York, 1988), p. 1327.
5. F. J. Margetan, R. B. Thompson, and T. A. Gray, Interfacial spring model for ultrasonic interactions with imperfect interfaces: theory of oblique incidence and application to diffusion bonded butt joints, submitted to J. Nondest. Eval.
6. Y. C. Angel and J. D. Achenbach, Reflection and transmission of elastic waves by a periodic array of cracks, J. Appl. Mech. 107: 33 (1985).